J Mater Sci: Mater Med (2006) 17:1003–1010
DOI 10.1007/s10856-006-0436-8

The use of advanced diffraction methods in the study of the structure of a bioactive calcia: silica sol-gel glass

Robert John Newport · Laura J. Skipper · Daniela Carta · David M. Pickup · Frank E. Sowrey · Mark E. Smith · Priya Saravanapavan · Larry L. Hench

Received: 8 November 2005 / Accepted: 3 February 2006

Abstract Sol-gel derived calcium silicate glasses may be useful for the regeneration of damaged bone. The mechanism of bioactivity is as yet only partially understood but has been strongly linked to calcium dissolution from the glass matrix. In addition to the usual laboratory-based characterisation methods, we have used neutron diffraction with isotopic substitution to gain new insights into the nature of the atomic-scale calcium environment in bioactive sol-gel glasses, and have also used high energy X-ray total diffraction to probe the nature of the processes initiated when bioactive glass is immersed *in vitro* in simulated body fluid. The data obtained point to a complex calcium environment in which calcium is loosely bound within the glass network and may therefore be regarded as facile. Complex multistage dissolution and mineral growth phases were observed as a function of reaction time between 1 min and 30 days, leading eventually, via octacalcium phosphate, to the formation of a disordered hydroxyapatite (HA) layer on the glass surface. This methodology provides insight into the structure of key sites in these materials and key stages involved in their reactions, and thereby more generally into the behaviour of bone-regenerative materials that may facilitate improvements in tissue engineering applications.

R. J. Newport (✉) · L. J. Skipper · D. Carta · D. M. Pickup · F. E. Sowrey
School of Physical Sciences, Ingram Building, University of Kent, Canterbury, CT2 7NH, UK
e-mail: r.j.newport@kent.ac.uk

M. E. Smith
Department of Physics, University of Warwick, Coventry, CV4 7AL, UK

P. Saravanapavan · L. L. Hench
Department of Materials, Imperial College London, London, UK, SW7 2AZ

1 Introduction

Melt-quenched silicate glasses containing calcium and phosphorus, and often alkali metals, have been much studied for their applications to promote bone regeneration and to bond to living bone, creating strong implants with less danger of interfacial instability than previous materials [1–4]. More recent work has focused on the use of the relatively low temperature sol-gel route for generating bioactive glasses, by which fewer components are required and a wider spectrum of compositions and glass porosities may be achieved. Samples of the general formula $(CaO)_x(SiO_2)_{1-x}$ have been shown to possess significant potential as bioactive bone-regenerative materials since they exhibit *Class A* bioactivity [3–7]. The exact mechanism by which these materials promote bone growth and the requirements for optimisation of their properties are still as yet only partially understood but have been strongly linked to evidence that gene activation necessary for tissue regeneration is linked to the release of soluble silica and calcium ions from the bioactive glass [6, 8]. A great deal of interest in the structure of these materials has therefore been engendered, particularly in the relationship between structure and bioactivity, and especially the nature and the role of the Ca sites within the glass network.

The local calcium environment in crystalline calcium silicate minerals and apatites is extremely diverse; in most minerals there are several crystallographically distinct Ca environments. This diversity, and thus the complexity, of environments is associated with a wide range of possible calcium-oxygen coordination numbers. Amorphous materials are intrinsically even more structurally complex in the sense that the long-ranged order of the crystalline form is lost. Analysis of the short-range environment in calcium silicate glasses has been attempted using X-ray absorption spectroscopy and X-ray powder diffraction [9–11], however

the complexity of the calcium environment limits the useful information available from these techniques. For instance, conventional diffraction measurements show the Ca–O correlations as a broad feature centred around 0.235 nm, but this feature is overlapped by the strong O–O correlation making a quantitative measure of Ca environment impossible based solely on such data.

1.1 Neutron diffraction with isotopic substitution (NDIS)

This technique offers the potential for the nature of the calcium environment to be probed in great detail, as studies of melt-quench derived silicate glasses have shown [12, 13]. In principle, it is possible with care to extract information on both short and medium-range order in such glassy materials using samples prepared with stable isotopes. However, there has hitherto been little such work published on the more subtle structures associated with the novel modified amorphous networks generated by the sol-gel method [14].

1.2 High energy X-ray diffraction (XRD)

Although our work is underpinned by a broad-based characterisation approach, combining complementary advanced physical probe techniques including neutron diffraction, X-ray absorption spectroscopy and multinuclear (^{29}Si, ^{17}O, ^{43}Ca) MAS NMR [15], the results reported herein are derived from X-ray diffraction (XRD) using the relatively short wavelengths and high fluxes available only from a synchrotron source. Electron diffraction has provided some evidence for there being a precursor to the deposition of hydroxyapatite on such bioactive glasses [16], but both electron diffraction and conventional laboratory-based XRD are limited by the dynamic range of the data (i.e. the Q-range, where $Q = 4\pi \sin\theta/\lambda$, with 2θ being the scattering angle and λ the wavelength) in that hydroxyapatite can be mis-identified as octacalcium phosphate given their similar peak positions in the Q-range accessible. Previous work has not been able to offer a definitive statement regarding whether the structure is actually hydroxyapatite or a related calcium phosphate. Further, these studies have focussed on a conventional search for identifiable Bragg diffraction peaks only: i.e. the amorphous component, which is often large, tends to be ignored—we here adopt a total XRD approach which utilises all the available data.

2 Experimental

The isotopically enriched samples needed for the NDIS experiment were synthesised from $^{44}CaCO_3$ (96 atom% enriched, Chemgas): this was converted to $^{44}Ca(NO_3)_2$ by titration with 2M nitric acid, the resulting hygroscopic solid was dried at 130°C until no further weight loss was observed. Calcium nitrate containing a natural mixture of Ca isotopes is available commercially (99% pure $Ca(NO_3)_2\,4H_2O$, Fisher Chemicals). Two samples of $(CaO)_{0.3}(SiO_2)_{0.7}$ were prepared [17], one containing natural Ca and the other ^{44}Ca (having cross sections for coherent neutron scattering of $\sigma_{coh} = 278$ fm^2 and $\sigma_{coh} = 25$ fm^2 respectively). The NDIS experiment relies upon the samples being absolutely identical in composition and structure, i.e. with the only difference between the samples being the isotopes of Ca present. Thus, both sample preparation and subsequent characterisation must be carried out with rigorous care to ensure that this condition has been met. Crucially, both samples were shown to be structurally equivalent using X-ray diffraction (Station 9.1, Synchrotron Radiation Source, UK; given that X-rays scatter from the electrons in a material and not the nucleus, the diffraction pattern is unaffected by the particular isotopic mixture present).

Samples of composition $(CaO)_{0.3}(SiO_2)_{0.7}$ were synthesised for the XRD experiment according to the method described in detail elsewhere [17]. Specimens were immersed in simulated body fluid, SBF, prepared using existing literature methods [5], and incubated at 36.5°C according to published procedures [18].

2.1 Calcium inclusion

FT-Raman spectroscopy was undertaken as a function of temperature during the formation of the bioactive CaO-SiO_2 glasses in order to study how the structure of the network changes with heat treatment. Raman analysis was carried out on the stabilised sol-gel sample using a system consisting of an Olympus BX40 microscope together with a Jobin Yvon model HR640 Raman Spectrometer, fitted with a 25 mW helium neon laser (which gave approximately 3 mW of light of wavelength 623.8 nm at the sample), and a liquid nitrogen cooled CCD multichannel detector. The data was adjusted to give the same background noise levels in all the spectra, so that the relative heights of the peaks could measure the change in the amount of chemical species present. Spectra were recorded for samples heated from 150 to 600°C.

2.2 Neutron diffraction with isotopic substitution

The GEM (general materials) diffractometer at the ISIS pulsed neutron source, Rutherford Appleton Laboratory, UK, allows data to be collected over an exceptionally wide dynamic range, with $Q_{max} \approx 600$ nm^{-1} [19]. Given that the resolution in real space may be expressed as $\Delta r \sim 2\pi/Q_{max}$, this ensures the very best chance of being able to differentiate between distinct but close bond lengths. Finely powdered samples were held in cylindrical vanadium containers. The ATLAS suite of programs was used for data

reduction and correction, which includes the subtraction of container and background scattering and the effects of absorption, multiple scattering and inelastic scattering events; the spectra are normalised to an absolute scale using the scattering profile from a cylindrical sample of vanadium [19].

A Q-space simulation of the structure factor is generated using the following equation

$$p(Q)_{ij} = (N_{ij}\omega_{ij}/C_j) \cdot (\sin QR_{ij}/QR_{ij}) \exp\left(-Q^2\sigma_{ij}^2/2\right) \quad (1)$$

where $p(Q)_{ij}$ is the pair function in reciprocal space (i.e. derived from the real-space model by Fourier transformation); N_{ij}, R_{ij} and σ_{ij} are the coordination number, atomic separation and disorder parameter respectively of atom i with respect to atom j; c_j is the concentration of atom j, and ω_{ij} is a weighting factor calculated from the relevant concentration and neutron scattering length data.

2.3 X-ray diffraction

X-ray diffraction data were collected on station 9.1 at the SRS Daresbury Laboratory, UK, using a two circle diffractometer. Data were collected in $\theta/2\theta$ scans at ambient temperature; the wavelength was calibrated to $\lambda = 0.04858$ nm. This wavelength was low enough to provide data to a value of wavevector transfer ($Q_{\max} \sim 220$ nm^{-1}, a value significantly higher than would be achievable using a conventional laboratory-based source). Finely powdered samples were packed into flat-plate containers, of 1 mm depth, and covered with thin polyimide windows. The analysis of the data to provide an interference function, $i(Q)$, follows the method outlined by Warren [20] and implemented by Pickup et al. [21]. Real-space pairwise atomic correlations may be generated by Fourier transformation of the interference function using the following generic relationship:

$$D(r) = 2/\pi \int Q.i(Q) \cdot \sin Qr.dr \quad (2)$$

It is important to note that, due to the inhomogeneous nature of the reacted samples and the fact that the correlation function represents an average over all pairwise terms, weighted by concentration and element-dependent X-ray form factors, the $D(r)$ may only be analysed quantitatively in the case of an unreacted sample; *relative* trends are however more easily derived for all samples.

3 Results and discussion

3.1 Neutron diffraction with isotopic substitution

The two neutron diffraction spectra were collected on the GEM diffractometer at the ISIS spallation neutron source at the Rutherford Appleton Laboratory, UK. The resultant interference function, the Structure Factor $i(Q)$, can reveal real-space structural information by Fourier transformation to give the corresponding total pair correlation function [18]

$$T(r) = T_0(r) + 2/\pi \int Q_i(Q)M(Q)\sin(Qr)d(Q) \quad (3)$$

where $T_0(r) = 4\pi r\rho_0(\Sigma_i c_i b_i)^2$ is the average density contribution (ρ^0 is the atomic number density, c_i is the fraction of element i and $b_i = (\sigma_{\text{coh}}/4\pi)^{1/2}$ is its associated coherent scattering length for neutron scattering) and $M(Q)$ is a Lorch modification function used to take into account the finite maximum experimentally attainable value of Q. Structural information is obtained from the neutron diffraction data by an iterative fitting of the $i(Q)$ using trial values for the real-space pair correlations [22].

Hence, if two experiments are performed in which the scattering length of element A is varied by isotopic substitution, the difference between the experimental correlation functions is of the form [23]

$$\begin{aligned}\Delta T(r) &= T(r) - T'(r) \\ &= c_A^2\left(b_A^2 - b_{A'}^2\right)t'_{AA'} + 2\sum c_A c_j b_j (b_A - b_{A'})t'_{Aj}(r)\end{aligned} \quad (4)$$

where $t'_{\text{AX}}(r)$ represents the partial pair correlation function for elements A and X. Thus, the structural environment of element A may be isolated using this method: in other words, in the present case, the result of taking the difference is that one is left with *only* the correlations involving Ca, all the other pairwise terms (e.g. Si—O) having been cancelled out. This powerful method therefore facilitates the quantitative study of the local atomic environment around the minority calcium species and thereby offers a unique insight into the structural role of the key element in these bioactive materials.

The $i(Q)$ of the $^{\text{nat}}$Ca and ^{44}Ca-enriched $(CaO)_{0.3}(SiO_2)_{0.7}$ samples are shown in Fig. 1, together with the corresponding weighted difference between the two. The structural parameters derived from fitting to the difference function are provided in Table 1 with additional information on the 'host' silica network derived from the original diffraction data and from complementary X-ray diffraction. The Fourier transform of the difference function, and the associated numerical fit using the parameters presented in Table 1, are shown in Fig. 2; this provides information exclusively on the Ca-X pair

Table 1 Fitting parameters obtained from simulation of neutron diffraction data

Correlation	R/nm ($\pm$ 0.001)	N ($\pm$ 0.25)	σ/nm ($\pm$ 0.1)
D—D	0.128	1.02	0.5
Si—O	0.161	3.8	0.5
Si—D	0.220	0.7	1.5
Ca—O	0.232	2.3	0.8
Ca—O	0.251	1.65	0.7
O—O	0.264	4.64	0.9
Ca—O	0.275	1.05	0.8
Ca—D	0.295	0.6	0.8

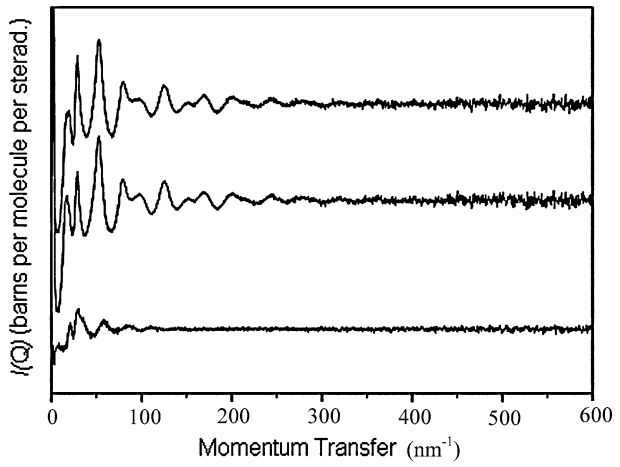

Fig. 1 $i(Q)$ data for ^{nat}Ca (top) and ^{44}Ca (middle) $(CaO)_{0.3}(SiO_2)_{0.7}$ and difference between $i(Q)$ functions from the ^{44}Ca and ^{nat}Ca samples. ^{nat}Ca and difference have been offset by $+0.2$ and -0.2 respectively for clarity

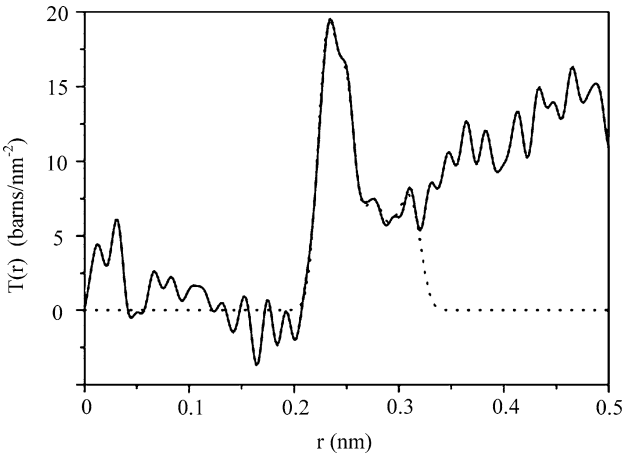

Fig. 2 Difference correlation function, $t_{Ca\text{-}X}(r)$, obtained by Fourier transformation of the difference between $i(Q)$ functions from the ^{44}Ca and ^{nat}Ca samples (*solid line*) and simulation of the $t_{Ca\text{-}X}(r)$ function (*dotted line*)

correlations present in the material. The slight ripple through the data is a residual artefact of the data analysis process.

The parameters obtained for Si—O and O—O are as one would expect for porous sol-gel derived silica [21] and this lends confidence to the fitting of the other correlations observed. In a fully condensed silica network the O—O coordination number would be 6; in these materials it is reduced to ~4.6 due to the presence of non-bridging oxygen atoms (NBO), which are abundant in high surface area materials due to the network modifying effects of the Ca cations and to the presence of network terminating hydroxyl groups. It is important also to note that the parameters obtained from the fit to the difference correlation function, $t_{Ca\text{-}X}(r)$, may be carried over to the fitting of the original datasets unchanged: we take this as further evidence that the fits generated to $t_{Ca\text{-}X}(r)$ are robust.

The fit parameters obtained uniquely from the NDIS results show clearly that the Ca–O environment actually consists of distinct, but partially overlapping, correlation shells centred at 0.23, 0.25 and 0.275 nm. This is the first time a Ca–O environment of this complexity has been discerned in the context of contemporary bioactive glass materials: it is a key observation given the central role that Ca dissolution plays in the material's ability to promote bone growth.

It is helpful at this point to draw comparisons with crystalline calcium silicate materials where Ca–O distances ranging from 0.23 to 0.28 nm have been observed, indicating that the values obtained here are certainly physically reasonable. In theory it should be possible to extract information from the NDIS data relating to higher correlations such as those from Ca–Si and Ca–Ca. However in practice, even using this method, the residual overlaps between the large range of possible correlations above ~0.3 nm renders this unreliable as a quantitative exercise. What the NDIS results do offer is the uniquely detailed quantitative data required for computer simulation studies of bioactive glasses, and in particular towards the full understanding of the Ca dissolution and subsequent mineral deposition processes.

3.2 X-Ray diffraction

The nature of the variation in overall composition of samples immersed in SBF has previously been measured using X-ray fluorescence: approximately 75% of the initial calcium content is lost from the sample within 30 min of reaction time, after which a gradual increase in Ca content occurs [24]. A key observation is that the Ca content undergoes a series of oscillations during the initial reaction period, before entering a long period of more monotonic increase thereafter. Analogous fluctuations in the calcium concentration within the SBF as a function of time have previously been observed for similar glasses immersed in SBF, along with corresponding fluctuations in the pH of the solution, but the fluctuations have not been explained [25]. Although not on identical samples, there are published results derived from the measurement of the zeta potential (which relates to the surface charge present on the solid bioactive material) that also reveal fluctuations over similar time periods [25]. One is drawn inexorably to

the conclusion that the fluctuations must be due to continual release of calcium from the glass and the growth of calcium phosphate on the glass surface. The dissolution of the bioactive glass, and the growth in its place of hydroxyapatite, cannot therefore be a monotonic process—and thus understanding the precise details of this process at the atomic scale will be helpful in optimising these materials. Indeed, the possibility that calcium phosphate-like phases are being formed and resorbed/transformed repeatedly as a function of SBF reaction time must be considered a distinct possibility (but one only open to study via diffraction methods if genuinely *in situ*/time-resolved experiments are designed and undertaken).

Conventional powder diffraction experiments typically focus on the observed Bragg peaks (in Q-space), and the analogous studies of amorphous materials focus on the diffuse pair correlation function (in real-, r-, space). Here, a total diffraction strategy is adopted [26] in which Bragg analysis in Q-space and Fourier analysis of the r-space pair distribution, to provide both crystallographic *and* local order information, are combined. The experimentally determined interference functions, $i(Q)$, for the unreacted and reacted samples are shown in Fig. 3. It is immediately apparent that, after only 30 min, the shape of the $i(Q)$ has altered significantly, most noticeably on the high-Q side of the first principal diffraction peak at $\sim$21 nm^{-1}; this change is associated with the initial rapid dissolution of Ca [5]. After 1 Hr, whilst the underlying amorphous pattern remains, there is clear evidence for the formation of Bragg diffraction peaks: i.e. of the growth of crystallites within the sample. The peaks observed at 5 h appear very strong (although the intensity may in part be the result of an inhomogeneity of crystallite concentration within the powder sample) and may be attributed to the presence of calcium phosphate. In particular, the two peaks at 28 and 94 nm^{-1}, seen only in the 1- and the 5-h spectra, are associated with the (412) and (200) reflections from octacalcium phosphate respectively (and not with hydroxyapatite) [16]. However, by 10 h the polycrystalline calcium phosphate appears to have been largely replaced by a more dominant disordered phase which, in its turn becomes increasingly prominent and well-defined thereafter. By 25 h, and even more clearly by 72 h, the $i(Q)$ has the appearance of a poorly crystalline hydroxyapatite overlaying a (Ca-depleted) silicate glass interference pattern. Given that hydroxyapatite recrystallises at $\sim$600°C, the 7-day sample was annealed in order to help verify its presence: the diffraction pattern readily sharpened to reveal the presence of polycrystalline hydroxyapatite.

The corresponding real-space pair correlation function, $D(r)$, allows us to consider the amorphous (short-range) component in more detail. Figure 4 shows the $D(r)$ curves for the untreated and the reacted samples. In order to bring out the important qualitative changes taking place, we have chosen to scale the various $D(r)$ such that the area of the Si—O first neighbour correlation, at 0.161 nm, is made the same for each. It is possible to discern four distinct changes that occurred with increasing exposure to SBF solution. The correlation at 0.202 nm, labelled as peak (a) in Fig. 4, was found as a major feature only in the SBF-reacted $(CaO)_{0.3}(SiO_2)_{0.7}$ sol-gel glasses and corresponds to the second neighbour O—H bond lengths found in hydrated

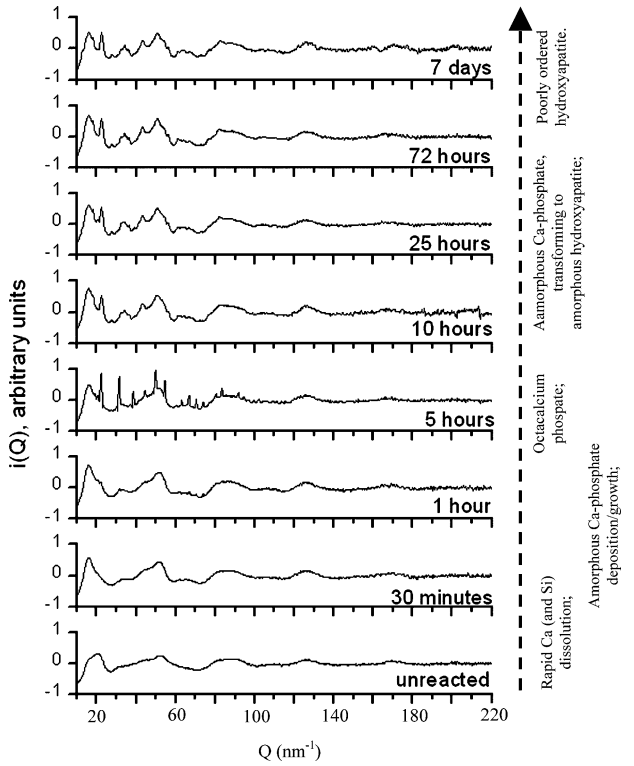

Fig. 3 $i(Q)$ data for SBF treated samples: from top to bottom, 7 days, 72 h, 25 h, 10 h, 5 h, 1 h, 30 min, unreacted

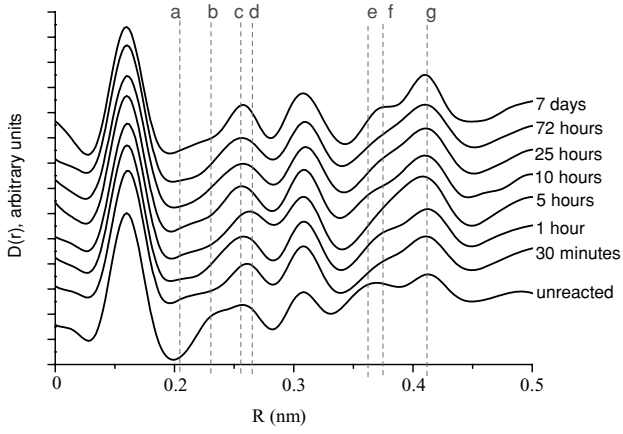

Fig. 4 $D(r)$ data for SBF treated samples: from top to bottom, 7 days, 72 h, 25 h, 10 h, 5 h, 1 h, 30 min, unreacted. In all cases the correlation functions have been normalised to the Si—O first-neighbour peak as it appears in the unreacted sample

calcium phosphates [27]. The correlation labelled peak (b) at 0.23 nm appears only in the unreacted sample: after exposure to SBF it disappears. Peak (c), at 0.254 nm, begins to change position on exposure to SBF, reaching a maximum correlation distance of 0.263 nm after 5 h, labelled peak (d). Similarly, peaks (e) and (f), at 0.36 and 0.375 nm respectively, also show a shift in their position; the peak at shorter r being replaced on SBF treatment by a feature at a longer correlation distance. Peak (g) at 0.408 nm narrows as the SBF reaction progresses. From a comparison with distances observed in calcium silicate minerals [28–30], peaks (b) and (c) may be assigned as Ca─O, and peak (e) with the corresponding higher order Ca─O, Ca─Ca and Ca─Si correlations. Peak (d) is within the range reported in the literature for the Ca─O bond in both calcium phosphates and hydroxyapatite [31] whereas (f) is most probably due to a combination of Ca─O─Ca, inter-tetrahedral P-O and intra-tetrahedral P─O─P peaks in hydroxyapatite. The decrease in intensity of peaks (b), (c) and (e) in the $D(r)$, and the associated increase in the intensity of peaks (d), (f) and (g), mirror in real-space the changes already identified in the interference patterns, $i(Q)$: that is to say the removal of Ca from the glass network and the growth of a calcium phosphate layer followed by an increasingly ordered form of hydroxyapatite. Given that the pair correlation function, $D(r)$, is an average over the volume of the sample in the X-ray beam—in contrast to the Bragg features observed in the $i(Q)$, which may derive from small crystallites at the glass surface—we surmise that the real-space data reveal a change in the underlying glass network structure, which may be correlated with the measured changes in the overall sample composition discussed above. The reported XRF analysis also revealed a decrease in phosphorus content at ∼5 h, to a value less than that observed at 30 min, which is reflected in the relative intensities of the inter-tetrahedral P─O and intra-tetrahedral P─O─P correlations observed at ∼0.37 nm.

This structural analysis provides additional supportive evidence for a dynamic reaction mechanism driven by the interplay between the pH of the SBF and the surface charge of the glass. Indeed, although, to our knowledge, it has not been directly observed with bioactive glasses before, octacalcium phosphate is not an unlikely phase to find given that it forms at a lower pH than hydroxyapatite, and so would be expected to form earlier where the pH was lower and thus prior to HA formation. Since HA is more thermodynamically stable than octacalcium phosphate, the latter might reasonably be expected to transform to HA. We have of course assumed both that the 'hydroxyapatite' is not a carbonated apatite—an assumption that seems to be supported by the annealing studies mentioned above and published elsewhere [32]—and that our $i(Q)$ are not rendered misleading by high levels of prefered crystal orientation associated with growth on the surface of the glass. The liklihood of prefered orientation is arguably significantly reduced when examining sol-gel samples simply because the glass surfaces themselves are not smooth, and in the case of the experiments reported here the samples were ground to powder before being placed in the neutron or X-ray beam.

3.3 Raman spectroscopy

The FT-Raman spectroscopy results are shown in Fig. 5. Calcium nitrate is one of the starting products of the sol-gel route of $CaO─SiO_2$ production, and the only peak present in the Raman spectra can be assigned to this nitrate ion, at 1052 cm^{-1}. Peaks for calcium oxide are not observed using Raman spectroscopy. The data has been normalised so that the height of the peak is proportional to the concentration

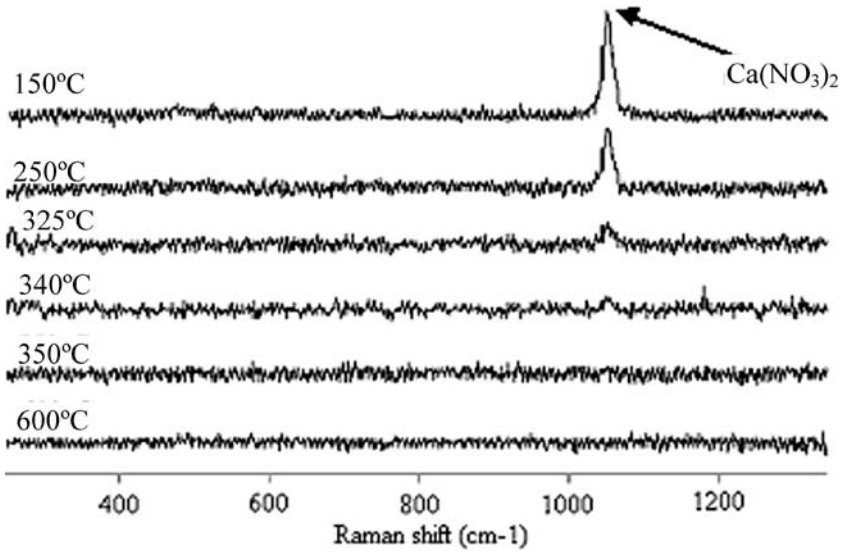

Fig. 5 Raman spectra of $(CaO)_x(SiO_2)_{1-x}$ $x = 0.3$ glass sample taken at various stages of heat stabilisation

of nitrate present [32]. At 250°C, the relative amount of nitrate present has reduced by half. The concentration of nitrate present continues to decrease rapidly up to 340°C until, after heating the sample up to 350°C, there is no peak visible. This is taken to mean that the calcium is in some other form—in other words, that it is not fully incorporated into the silica host network until ∼350°C. This is suggestive of a relatively weak bonding within the silica host network.

4 Conclusions

In summary, by using neutron diffraction with isotopic substitution we have observed directly three Ca─O distances in a bioactive $(CaO)_x(SiO_2)_{1-x}$ sol-gel glass and quantified their respective contributions to the bonding of Ca within the silica network. The data obtained point to a complex calcium environment in which the calcium is loosely bound at the surface of the network. This data provides a direct atomic-scale explanation for the empirical observation that calcium loss from these materials is facile and can be achieved by simple ion exchange with body fluid. This is indirectly supported by the Raman data taken during sample synthesis.

We have also demonstrated the nature of the principal stages to the generation of HA on the surface of a bioactive glass. Further, a link has been demonstrated between these distinct structural stages and the macroscopically determined elemental analysis of the glass as a function of time; that is to say, the atomic-scale structure to the surface charge- and pH-driven dissolution/growth processes have been related. Following immersion of a sol-gel derived bioactive glass in body fluid there is rapid initial dissolution of Ca, there is a growth of an amorphous, or very poorly crystalline, calcium phosphate layer within 1 h of immersion, which becomes increasingly evident and/or ordered by 5 h. This more ordered phase is shown to be octacalcium phosphate. However, by 10 h this polycrystalline layer is apparently replaced by a predominantly disordered material, now more akin to an amorphous hydroxyapatite; it is this layer that then develops steadily into a more ordered, bone mineral-like, hydroxyapatite.

Although these observations pertain to a particular bioactive material, it is reasonable to suggest that the underlying mechanisms may have a high degree of commonality with those associated with other bioactive, tissue-regenerative, solids—and certainly that the experimental methodology for their investigation requires the generic breadth employed here. It is only by such a detailed knowledge of the sites of importance in complex materials that systematic improvements in their application to tissue engineering applications can be achieved.

Acknowledgments We are grateful to V FitzGerald for her help in the collection of the neutron data, and to our referees for their particularly useful suggestions. We acknowledge the support of the EPSRC (awards GR/R57492 and GR/R59298) and of the CCLRC (SRS and ISIS facilities, and their instrument scientists), the University of Kent Hyatt-Wolff fund for a studentship (LJS) and also the EPSRC/ESRF for a studentship (KOD).

References

1. L. L. HENCH and J. WILSON, "Introduction to Bioceramics" (World Scientific, Singapore, 1993).
2. L.L. HENCH, *Biomaterials* **19** (1998) 1419.
3. R. LI, A. E. CLARK and L. L. HENCH, "Chemical Processing of Advanced Materials" (Wiley, New York, 1992).
4. M. M. PEREIRA, A. E. CLARK and L. L. HENCH, *J. Mater. Synth. Proc.* **2** (1994) 189.
5. P. SARAVANAPAVAN, J. R. JONES, R. S. PRYCE and L. L. HENCH, *J. Biomed. Mat. Res. A*. **66A** (2003) 110.
6. P. SARAVANAPAVAN, S. VERRIER, J. R. JONES, R. BEILBY, V. J. SHIRTLIFF, L. L. HENCH and J. M. POLAK, *Bio-Med. Mater. Eng.* **14** (2004) 467.
7. M. CERRUTI, G. MAGNACCA, V. BOLIS and C. MORTERRA, *J. Mater. Chem.* **13** (2003) 1279.
8. I. D. XYNOS, A. J. EDGAR, L. D. K. BUTTERY, L. L. HENCH and J. M. POLAK, *J. Biomed. Mater. Res*. **155** (2000) 151.
9. F. E. SOWREY, L. J. SKIPPER, D. M. PICKUP, K. O. DRAKE, Z. LIN, M. E. SMITH and R. J. NEWPORT, *Phys. Chem. Chem. Phys*. **6** (2004) 188.
10. L. J. SKIPPER, F. E. SOWREY, D. M. PICKUP, V. FITZGERALD, R. RASHID, K. O DRAKE, Z. LIN, P. SARAVANAPAVAN, L. L. HENCH, M. E. SMITH and R. J. NEWPORT, *J. Biomed. Mater. Res.* **70A** (2004) 354.
11. L. J. SKIPPER, F. E. SOWREY, D. M. PICKUP, R. J. NEWPORT, K. O. DRAKE, Z. LIN, M. E. SMITH, P. SARAVANAPAVAN and L. L. HENCH, *Mater. Sci. Forum.* **480–481** (2004) 21.
12. M. C. ECKERSLEY, P. H. GASKELL, A. C. BARNES and P. CHIEUX, *Nature* **335** (1988) 6190.
13. P. H. GASKELL, M. C. ECKERSLEY, A. C. BARNES and P. CHIEUX, *ibid.* **350** (1991) 6320.
14. D. M. PICKUP, F. E. SOWREY, R. J. Newport, P. N. GUNAWIDJAJA, K. O. DRAKE and M. E. SMITH, *J. Phys. Chem. B* **108** (2004) 10872.
15. Z. LIN, M. E. SMITH, F. E. SOWREY and R. J. NEWPORT, *Phys. Rev. B* **69** (2004) art. No. 224107.
16. Y. LENG, X. LU and J. CHEN, *Key Eng. Mater.* **254–256** (2004) 339.
17. P. SARAVANAPAVAN and L. L. HENCH, *J. Non-Crys. Solids* **318** (2003) 1.
18. P. SARAVANAPAVAN and L. L. HENCH, *J. Biomed. Mater. Res.* **54** (2001) 608.
19. A. C. HANNON, *Nucl. Instrum. Methods Phys. Res. A* **551** (2005) 88.
20. B. E. WARREN, "X-Ray Diffraction" (Dover Publications Inc., New York, 1990).
21. D. M. PICKUP, G. MOUNTJOY, M. A. ROBERTS, G. W. WALLIDGE, R. J. NEWPORT and M. E. SMITH, *J. Phys.: Condens. Mater.* **12** (2000) 3521.
22. P. H. GASKELL, "Materials Science and Technology," vol. 9. (VCH, Weinhaim, 1991).
23. C. A. YARKER, P. A. V. JOHNSON, A. C. WRIGHT, J. WONG, R. B. GREEGOR, F. W. LYTLE and R. N. SINCLAIR, *J. Non-Cryst. Solids* **79** (1986) 117.

24. L. J. SKIPPER, F. E. SOWREY, R. J. NEWPORT, Z. LIN and M. E. SMITH, *Phys. & Chem. Glasses* **46** (2005) 372.
25. T. KOKUBO, H-M. KIM and M. KAWASHITA, *Biomaterials* **24** (2003) 2161.
26. S. J. HIBBLE, A. C. HANNON and I. D. FAWCETT, *J. Phys.: Condens. Matter*. **11** (1999) 9203.
27. N. S. MANDEL, *Acta Crystallogr. Sect. B: Struct. Sci.* **B31** (1973) 1730.
28. K. S. MAMEDOV and N. V. BELOV, *Dokl. Akad. Nauk* **107** (1956) 465.
29. T. ITO, R. SADANAGA, Y. TAKEUCHI and M. TOKONAMI, *Proc. Japan Acad.* **45** (1969) 913.
30. Y. OHASHI, *Phys. Chem. Miner.* (Germany) **10** (1984) 217.
31. R. M. WILSON, J. C. ELLIOT and S. E. P. DOWKER, *Am. Min.* **84** (1999) 1406.
32. L. J. SKIPPER, F. E. SOWREY, R. J. NEWPORT, Z. LIN and M. E. SMITH, *Phys. & Chem. Glasses* **46** (2005) 372.